Influence of particle size distribution on random close packing of spheres

Kenneth W. Desmond and Eric R. Weeks

Department of Physics, Emory University, Atlanta, Georgia 30322, USA

The densest amorphous packing of rigid particles is known as random close packing. It has long been appreciated that higher densities are achieved by using collections of particles with a variety of sizes. For spheres, the variety of sizes is often quantified by the polydispersity of the particle size distribution: the standard deviation of the radius divided by the mean radius. Several prior studies quantified the increase of the packing density as a function of polydispersity. A particle size distribution is also characterized by its skewness, kurtosis, and higher moments, but the influence of these parameters has not been carefully quantified before. In this work, we numerically generate many sphere packings with different particle radii distributions, varying polydispersity and skewness independently of one another. We find that the packing density can increase significantly with increasing skewness and in some cases skewness can have a larger effect than polydispersity. However, the packing fraction is relatively insensitive to the higher moment value of the kurtosis. We present a simple empirical formula for the value of the random close packing density as a function of polydispersity and skewness.

I. INTRODUCTION

Understanding various aspects of random close packing (RCP) has great scientific and industrial importance [1] as it has been linked to a wide range of problems such as the structure of living cells [2], liquids [3,4], granular media [5–8], emulsions [9], glasses [10], amorphous solids [11], jamming [12,13], the viscosity of suspensions [14,15], and the processing of ceramic materials [16]. Random close packing is typically defined as a collection of particles packed into the densest possible amorphous configuration, although more rigorous definitions are available [17]. Experiments found that the densest random packing of monodisperse spheres typically occurs close to $\phi_{0,\mathrm{RCP}} \sim 0.64$ [4], where the density ϕ (or packing fraction) is defined as the ratio of the total volume occupied by spheres to the volume of the container.

Formally, a packing consists of particles with a distribution in radii $P(R)$. The polydispersity is defined as

$$\delta = \sqrt{\langle \Delta R^2 \rangle}/\langle R \rangle. \tag{1}$$

Here, $\Delta R = R - \langle R \rangle$ and the moments of R (and ΔR) are defined as $\langle R^n \rangle = \int R^n P(R) dR$ [and $\langle \Delta R^n \rangle = \int \Delta R^n P(R) dR$]. It has long been appreciated that packings of spheres can have larger RCP densities when $\delta > 0$ [18–23]. Prior experiments [24–28] and simulations [29–33] have nicely shown that as the polydispersity increases, the particles pack to higher-volume fractions because the smaller particles pack more efficiently by either layering against larger particles or by fitting into the voids created between neighboring large particles [21,25,34,35]. In practice, depending on the degree of the polydispersity, the packing fraction can increase from 0.64 for monodisperse packings to nearly ~ 0.75 for packings with 0.65 polydispersity [25]. For the extreme case of two different particle sizes with a size ratio approaching infinity, the voids between the large particles can be packed randomly with small particles and so ϕ can be as large as $\phi_{0,\mathrm{RCP}} + (1 - \phi_{0,\mathrm{RCP}})\phi_{0,\mathrm{RCP}} \approx 0.88$ [35,36].

While it is intuitive that the polydispersity can affect ϕ_{RCP}, it is also reasonable that the shape, not just the spread, of the distribution $P(R)$ may also influence ϕ_{RCP} [1,25]. For instance,

an infinite number of distributions can have the same value of δ but yet differ in their form. One can characterize the shape using the skewness

$$S = \langle \Delta R^3 \rangle/\langle \Delta R^2 \rangle^{3/2}, \tag{2}$$

kurtosis

$$K = \langle \Delta R^4 \rangle/\langle \Delta R^2 \rangle^2, \tag{3}$$

and higher moments. There have been prior studies that have investigated the influence of distribution shape on the density of tightly packed particles [16,25,35,37–41]. Similar to the studies on polydispersity, they find that the shape of the particle distribution can have a profound influence on the packing density. However, these prior studies either did not independently vary δ and S but rather conflated the influences of both, or else used other metrics besides δ and S to quantify $P(R)$. Of the prior studies, Tickell *et al.* [42] is the only one to report on the effects of skewness and kurtosis for experiments carried out with sand, finding that over a narrow range in skewness the packing density can increase by 0.04 with no dependence on kurtosis. However, they did not control for polydispersity, leaving unclear the relative importance of polydispersity and skewness. The key unanswered question by the prior work is how the skewness of a distribution influences ϕ_{RCP}, and how large this effect is relative to the effects of polydispersity.

In this paper, we address this question by numerically generating packings with a variety of particle-size distributions. We find that both polydispersity δ and skewness S influence the maximum random close packing volume fraction. In particular, increasing δ increases ϕ_{RCP}, and for a given δ, ϕ_{RCP} increases linearly with increasing S. As S can be negative, a negatively skewed $P(R)$ can decrease ϕ_{RCP} as compared to a symmetric distribution. We find no universal influence of the kurtosis on our results.

II. PROTOCOL

Packings of arbitrary size distributions $P(R)$ are generated using a numerical protocol, with a goal of controlling δ and

S independently. Our method for generating these packings was previously developed in Ref. [43]. Briefly, infinitesimal particles are placed randomly in a periodic container, gradually expanded, and moved at each step to prevent particles from overlapping. At the beginning of the simulation, particles are assigned radii with a specific distribution and as the particles expand they do so by a multiplicative factor such that the shape of the radii distribution is fixed. The value of ϕ_{RCP} is known to be sensitive to protocol [44,45], and it is not known if this algorithm or any other algorithm produces rigorously defined random close packed states [13,17,43,46]. Our goal is not to determine the precise value of ϕ_{RCP} for a given $P(R)$ but rather to empirically understand the trend in ϕ_{RCP} with polydispersity and skewness. Happily, our algorithm when applied to a monodisperse packing gives $\phi_{0,\text{RCP}} \sim 0.64$, close to the experimentally found value and in agreement with prior simulation work. In practice, the simulation has three adjustable parameters that determine how quickly the simulation converges to a RCP state. These parameters are the initial packing fraction, the rate of expansion and contraction, and a threshold on the minimum energy (see Ref. [47] for more details). We use the same values as in Ref. [47], and we find that our algorithm produces reproducible results and ϕ_{RCP} is not sensitive to slight changes in these values.

To efficiently determine ϕ_{RCP} for a chosen particle-size distribution, we exploit the known finite-size dependence $\phi_{\text{RCP}}(h) = \phi_{\text{RCP}}^{\infty} - C/h$, where h is the system size, $\phi_{\text{RCP}}^{\infty}$ is the random close packing fraction in the limit $h \to \infty$, and C is a fitting constant [47]. By generating many packings with different periodic box sizes h, we fit $\phi_{\text{RCP}}(h)$ to determine $\phi_{\text{RCP}}^{\infty}$ for each distribution. We generate packings with box sizes of ~10, 14, 18, and 23 mean particle diameters in length to determine $\phi_{\text{RCP}}^{\infty}$. For the rest of the paper, ϕ_{RCP} will be used to indicate $\phi_{\text{RCP}}^{\infty}$.

To control for both δ and S independently, we study packings using four different distributions: binary, linear, Gaussian, and lognormal. The binary and linear distributions are determined by two control parameters, allowing for us to control δ and S independently, while the Gaussian and lognormal distributions are determined by only one parameter, and therefore δ and S cannot be controlled independently. By generating many packings with different δ and S using these four distributions, we can compare the results to see how sensitive ϕ_{RCP} is to polydispersity and skewness, but we can also compare different distributions with the same δ and S to see how sensitive ϕ_{RCP} is to other subtle differences in the distribution shape. For all distributions, we impose $\langle R \rangle = 1$.

More specifically, the binary distribution consists of particles with two distinct radii. The shape of the distribution is determined by the size ratio and number ratio of these two particle types. The linear distribution is a continuous distribution of the form $P(R) = AR + B$, where the distribution in particle size exists over a finite range $a \leqslant R \leqslant b$. Our choice of $\langle R \rangle = 1$ and the requirement of normalization $[\int_a^b P(R)dR = 1]$ imposes two constraints on the parameters (a,b,A,B). For the two remaining degrees of freedom, we define $\eta = b/a$ and $\rho = P(b)/[P(a) + P(b)]$. We compute S and δ for a grid of η and ρ values and then interpolate to find the parameters for $P(R)$ for the desired S and δ values, allowing us to vary them systematically. The third distribution

is a Gaussian of the form $P(R) = A_G \exp[-(R-1)^2/2\sigma^2]$, where σ is the standard deviation and $A_G = 1/(\sqrt{2\pi\sigma^2})$. For larger σ, some of the particle radii could be negative, which is unphysical, or very close to zero, which may prevent generating packings within a reasonable time frame. To avoid these issues, we truncate the Gaussian distribution such that the smallest particle radius is no smaller than 0.1. The Gaussian distribution has a fixed skewness $S = 0$ except for the truncated Gaussians, which have a slight positive skewness. The last distribution we consider is the lognormal distribution $P(R) = A_L \exp\{-0.5[\ln(R)/\sigma + 0.5\sigma]^2\}/R$, where $A_L = 1/(\sqrt{2\pi\sigma^2})$. Similar to the Gaussian distribution, the skewness of the lognormal distribution is not adjustable but is always positive and becomes larger as σ becomes larger. We provide a summary of the distributions in Table I.

III. RESULTS AND DISCUSSION

In Fig. 1(a), we compare three different distributions with polydispersity $\delta = 0.25$ and nearly the same positive skewness $S \approx 0.75$. We see that the distributions are quite different, in particular in their tails. For example, the linear distribution has more small particles than the other two distributions. The lognormal distribution has tails that include both smaller and larger particles than the other two distributions. It's not necessarily obvious how the values of ϕ_{RCP} will be ranked for these cases. In Fig. 1(b), we show two different distributions with polydispersity $\delta = 0.25$ and skewness $S \approx -0.5$. As these distributions have negative skewness, both distributions have more larger particles than smaller particles. Once again, it's not necessarily clear how ϕ_{RCP} should differ between the two packings.

After generating nearly 10 000 packings with different particle radii distributions, we plot ϕ_{RCP} as a function of skewness S for all our data in Fig. 2, with the different groups of data (different colors) corresponding to different polydispersity values δ. Each data point in the figure has a one to one correspondence to the distribution type, δ, and S. The symbol or line type of the data indicates the $P(R)$ distribution type. Remarkably, the figure shows that regardless of the type of particle radii distribution, ϕ_{RCP} is nearly the same for the same pairing of polydispersity and skewness. It also shows that ϕ_{RCP} increases with both increasing δ and S. Strikingly, the skewness can have an equally important effect as the polydispersity. For example, for $\delta = 0.40$ and $S = 0$, ϕ_{RCP} is shifted upward by ≈ 0.02. Fixing that value of δ, changing S to ± 1 shifts ϕ_{RCP} by $\approx \pm 0.02$. For highly polydisperse samples, one cannot accurately know ϕ_{RCP} without also knowing the skewness of the radius distribution. For the binary samples (solid lines in Fig. 2), S can be even larger in magnitude and have an even larger influence on ϕ_{RCP} than δ has.

The increase in ϕ_{RCP} with skewness is not uniform. For negative skewness (more big particles), the polydispersity δ does not seem to influence ϕ_{RCP} as much as when the skewness is positive. This is not too surprising since the volume of each particle grows with R^3. When the total number of bigger particles is greater than the total number of smaller particles (negative skewness), the volume occupied by all the large particles is significantly greater than the

TABLE I. Summary of the distributions $P(R)$ tested. The functional form of $P(R)$ is shown in the first row. The free parameters governing the shape of $P(R)$ are shown in the next set of rows. Each distribution is constrained such that $\langle R \rangle = 1$ and the probability distribution is normalized to unity, which constrains some of the coefficients in $P(R)$ to fixed values, listed as "Constrained" in the table. The last rows list the polydispersity, skewness, and kurtosis for each distribution. For the binary distribution, $\delta(R)$ is the Dirac delta function. For the linear distribution, analytic solutions are complicated for δ, S, and K and so are computed numerically. For the Gaussian and lognormal distributions, a truncation was applied to ensure that no particle radii were below 0.1. This affects the shape slightly, and the δ, S, and K were computed numerically when truncation was applied.

Binary

Function	$P(R) = (1-\rho)\delta(R-a) + \rho\delta(R-b)$
Parameters	Number fraction $\rho = P(b)/[P(a)+P(b)]$
	Size ratio $\eta = b/a$
Constrained	$a = 1/(1-\rho+\eta\rho)$
	$b = \eta/(1-\rho+\eta\rho)$
Polydispersity	$\delta = [(1-\rho)(a-1)^2 + \rho(b-1)^2]^{1/2}$
Skewness	$S = [(1-\rho)(a-1)^3 + \rho(b-1)^3]/\delta^3$
Kurtosis	$K = [(1-\rho)(a-1)^4 + \rho(b-1)^4]/\delta^4$

Linear

Function	$P(R) = AR + B, \ a \leqslant R \leqslant b$
Parameters	Number ratio $\epsilon = P(b)/P(a)$
	$\eta = b/a$
Definitions	$c = 2(\epsilon-1)/[(\eta-1)^2(\epsilon+1)]$
	$d = 2/[(\eta-1)(\epsilon+1)] - c$
	$e = [c(\eta^3-1)/3 + d(\eta^2-1)/2]$
Constrained	$a = 1/e, b = \eta/e, A = ce^2, B = de$
Polydispersity	Solved numerically
Skewness	Solved numerically
Kurtosis	Solved numerically

Gaussian

Function	$P(R) = Ae^{-(R-1)^2/2\sigma^2}$
Parameters	Standard deviation σ
Constrained	$A = 1/\sqrt{2\pi\sigma^2}$
Polydispersity	$\delta = \sigma$
Skewness	$S = 0$
Kurtosis	$K = 0$

Lognormal

Function	$P(R) = \frac{A}{R}e^{[(\ln R)/\sigma + 0.5\sigma]^2/2}$
Parameters	Scale parameter σ
Constrained	$A = 1/\sqrt{2\pi\sigma^2}$
Polydispersity	$\delta = \sqrt{e^{\sigma^2}-1}$
Skewness	$S = (e^{\sigma^2}+2)\sqrt{e^{\sigma^2}-1}$
Kurtosis	$K = e^{4\sigma^2} + 2e^{3\sigma^2} + 3e^{2\sigma^2} - 3$

volume occupied by all the small particles. In effect, the big particles pack like a low-polydispersity sample and occupy the majority of the container, while the small spheres occupy an insignificant portion, and ϕ_{RCP} approaches $\phi_{0,RCP} \approx 0.64$ for a monodisperse sample. For positive skewness (more smaller particles), ϕ_{RCP} has a fairly strong dependence on δ and S, where ϕ_{RCP} increases with increasing number of small particles. The reason for this increase in ϕ_{RCP} is likely due to the small particles fitting into the spaces between larger particles. As discussed in prior work [21,25,35], the local porosity is
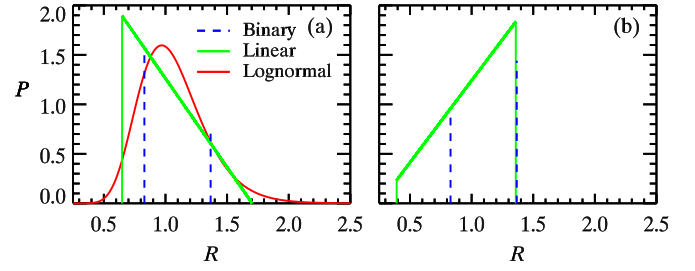

FIG. 1. (Color online) (a) Examples of three different particle radii distributions with the same polydispersity of 0.25 and nearly the positive same skewness. The binary distribution has $S = 0.78$, the linear distribution has $S = 0.56$, and the lognormal distribution has $S = 0.78$. (b) Examples of two different particle radii distributions with the same polydispersity of 0.25 and negative skewness $S = -0.5$.

smaller around two neighboring particles of different sizes than around two neighboring particles of the same size. This effect is greater for larger differences in the size of two neighbors. As skewness and polydispersity increase, both the number of small particles present and the average size discrepancy between neighboring particles increase, resulting in a larger ϕ_{RCP}.

To provide a qualitative sense of the behavior, Fig. 3 shows a 2D slice through four different 3D packings. Figures 3(a) and 3(b) are lognormal packings, where Fig. 3(a) is a packing at low polydispersity and skewness and Fig. 3(b) is a denser packing at a higher polydispersity and skewness. Packings in Figs. 3(c) and 3(d) are two binary packings with polydispersity 0.4, where Fig. 3(c) has a large negative skewness and Fig. 3(d) is denser and has a large positive skewness. As discussed above, at large δ and S, small particles can either layer around larger particles and/or fit in the voids between bigger particles. In Figs. 3(b) and 3(d) we see evidence of small particles sitting in the void areas between big particles. In Figs. 3(a) and 3(c),
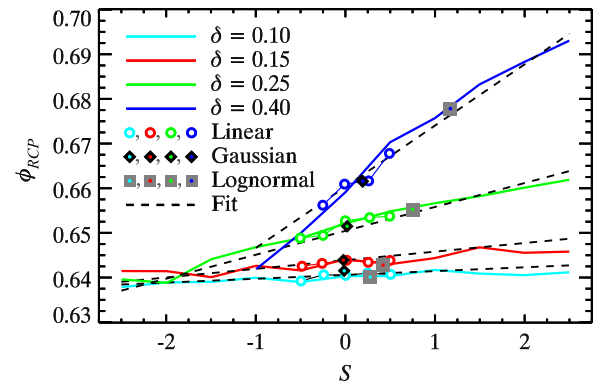

FIG. 2. (Color online) This figure shows how ϕ_{RCP} depends on particle-size distribution, polydispersity δ, and skewness S. The solid lines represent ϕ_{RCP} for binary packings and the symbols represent ϕ_{RCP} for packings with either linear, Gaussian, or lognormal particle distributions as indicated by the legend. The colors represent different polydispersities of either 0.1, 0.15, 0.25, or 0.4. The dashed lines are a fit to the data using $\phi_{RCP} = \phi_{RCP}^* + c_1\delta + c_2 S\delta^2$, where $\phi_{RCP}^* = 0.634$, $c_1 = 0.0658$, and $c_2 = 0.0857$.

Lognormal
$\delta = 0.106$, $S = 0.440$
$\phi = 0.640$ (a)

Lognormal
$\delta = 0.424$, $S = 1.36$
$\phi = 0.678$ (b)

Binary
$\delta = 0.401$, $S = -0.994$
$\phi = 0.642$ (c)

Binary
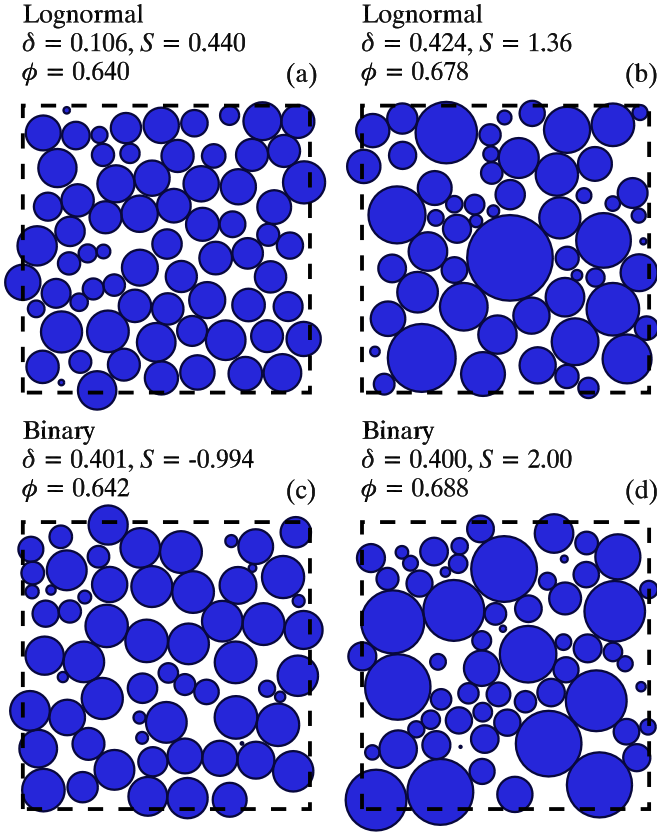$\delta = 0.400$, $S = 2.00$
$\phi = 0.688$ (d)

FIG. 3. (Color online) Each image represents a 2D slice through a 3D packing, and the dashed box is the boundary of the periodic packing. The volume fraction for each packing shown is close to the extrapolated ϕ_{RCP}. Also, the area fraction of each 2D slice is the same as the volume fraction of the 3D packing they represent. For each packing, the particle radii are randomly selected from a specified distribution with an exact δ and S. However, when choosing a finite number of particle sizes from one of these distributions, the particle-size distribution of the finite packing may be slightly different resulting in a slightly different δ and S. In this figure, we report δ, S, and ϕ for the finite packing shown, not the values used to randomly select the particle sizes.

where the skewness is lower, we see less evidence of this. These observations are consistent with the results described in the legend of Fig. 2.

Since ϕ_{RCP} is nearly determined by the two parameters δ and S, we fit all the data to a simple equation,

$$\phi_{\mathrm{RCP}} = \phi_{\mathrm{RCP}}^* + c_1\delta + c_2 S\delta^2, \qquad (4)$$

where $\phi_{\mathrm{RCP}}^* = 0.634$ is the packing fraction for a monodisperse packing of spheres ($\delta = 0$ and $S = 0$) and $c_1 = 0.0658$ and $c_2 = 0.0857$ are empirical constants. These fit lines are shown as dashed lines in Fig. 2 and agree reasonably well with the data. Our fitted value of ϕ_{RCP}^* is close to the experimentally accepted value of 0.637 [1,48]. We also tried fits with higher-order terms in S and δ, but we found first order in S and second order in δ reasonably fit all the data well.

There are slight differences in the ϕ_{RCP} values for different distribution types for the same δ and S values, seen in Fig. 2. Thus far we have focused on δ and S to characterize our
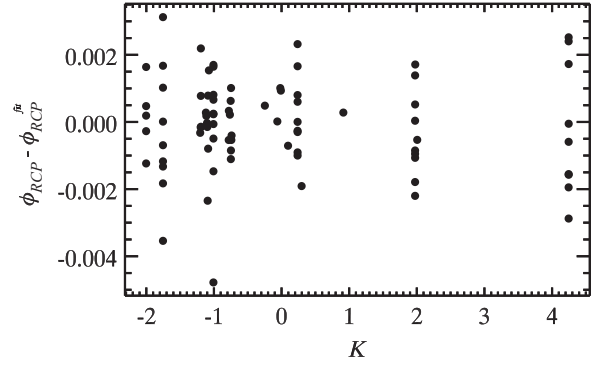

FIG. 4. The difference between ϕ_{RCP} and the fitted values $\phi_{\mathrm{RCP}}^{\mathrm{FIT}}$ in Eq. (4) are plotted as a function of kurtosis.

distributions, and of course the distributions differ in their higher moments. The next quantity to consider is the kurtosis K defined above [Eq. (3)], and it might be a potential additional parameter to explain the variations in Fig. 2. To check this, we subtract the computationally found values of ϕ_{RCP} from the empirical fit [Eq. (4)] and plot these differences as a function of K in Fig. 4, which shows no systematic dependence on K. That is, K seems not to be a useful fit parameter for ϕ_{RCP}. This agrees with the 1933 qualitative observations of Tickell *et al.* [42]. We also note that Fig. 4 demonstrates the quality of Eq. (4) to capture the actual value of ϕ_{RCP}. The figure shows that the fit typically is within 0.002 of the actual ϕ_{RCP} for nearly all the values of δ and S tested. The average absolute difference between the actual ϕ_{RCP} and the fitted ϕ_{RCP} is 0.001.

It is worth noting that our results apply to randomly packed objects, and one can consider other amorphous packings that are perhaps less random. For example, an important class of these are random Apollonian packings (RAP) [49,50]. To generate a RAP, one first places the largest spheres, then smaller particles are inserted into the voids between the spheres. For example, one can fill the voids with the largest possible spheres [49], which leads to a packing with a volume fraction approaching arbitrarily close to 1.0. In such situations, $P(R)$ is a power law, $P(R) \sim R^{-\alpha}$ for $R > R_0$, where R_0 is a cutoff. As R_0 approaches 0 (an infinite amount of iterations of the RAP protocol), the volume fraction approaches 1.0. Using our equations, you can see that if $R_0 = 0$, $\langle R^n \rangle$ is infinite for $n \geqslant \alpha - 1$. For finite but small R_0, $\langle r^n \rangle$ can be quite large, and thus the packing can have large values for δ, S, and K. Clearly in such limits the volume fraction nonetheless is 1.0 or smaller, so our empirical formula Eq. (4) must break down. On the other hand, the RAP protocols all ensure large volume fractions by construction—that is, the small particles are precisely chosen to fit into the voids between the large ones, and $P(R)$ is determined after the fact through the algorithm. Our computational algorithm will generally find less optimal packings for the same $P(R)$, and so it is to be expected that Eq. (4) should not apply to RAP.

For that matter, our algorithm converges unacceptably slowly for distributions with particle sizes varying by more than a factor of ten between the smallest and largest sizes, preventing us from directly testing power law packings. We work around this by using the numerical algorithm proposed by Farr and Groot [36], which rapidly predicts ϕ_{RCP} based on

any $P(R)$ as input. The predictions of their algorithm agree well with the results from our computed 3D packings for the distributions listed in Table I. We use their algorithm to determine ϕ_{RCP} for a variety of power law distributions over the same range of δ and S tested for our other distributions, and we find excellent agreement with our empirical expression, Eq. (4).

IV. CONCLUSIONS

Our data have two significant conclusions. First, the skewness S has a significant influence on ϕ_{RCP} for distributions with a large polydispersity δ. Second, Eq. (4) allows one to determine ϕ_{RCP} to within approximately ± 0.002 from knowing δ and S, without taking into account any other details of the shape of $P(R)$. We note that a very recent paper argues that ϕ_{RCP} is a simple function of $\langle R \rangle \langle R^3 \rangle / \langle R^2 \rangle^2$, using an inferred equation of state of hard sphere mixtures [51]. One could express their result in terms of δ and S, which gives a quite different expression from our results. Their function predicts ϕ_{RCP} to within ± 0.02. Our formula [Eq. (4)] yields a more accurate prediction, but is from an empirical approach rather than a physical approach.

This collapse of ϕ_{RCP} values for a given δ and S but different distribution shapes is intriguing, as presumably the structures within the packings are different for different $P(R)$. For that matter, one can have the same ϕ_{RCP} value for different δ and S, see for example Figs. 3(a) and 3(c), and clearly these will have different microstructures. This might be useful for studying aspects of the jamming transition of spherical particles. Many prior results show that various properties of these systems depend on the distance to the jamming point [52–56], where the jamming point is thought to be the same as ϕ_{RCP} [12,13,17,46]. One can imagine conducting experiments or simulations to compare the properties of packings near the jamming transition with different microstructures but the same jamming point. These could be equally useful for studying the colloidal glass transition, which may be influenced by ϕ_{RCP} [54,57–61]. Such experiments may provide further insight into the universal nature of the jamming transition and glass transition, but may also highlight subtle dependencies on the microstructure.

ACKNOWLEDGMENTS

[1] S. Torquato and F. H. Stillinger, Rev. Mod. Phys. **82**, 2633 (2010).

[2] T. M. Truskett, S. Torquato, and P. G. Debenedetti, Phys. Rev. E **62**, 993 (2000).

[3] O. K. Rice, J. Chem. Phys. **12**, 1 (1944).

[4] J. D. Bernal and J. Mason, Nature **188**, 910 (1960).

[5] W. O. Smith, P. D. Foote, and P. F. Busang, Phys. Rev. **34**, 1271 (1929).

[6] S. F. Edwards, *Granular Matter* (Springer-Verlag, Berlin, 1994).

[7] C. Radin, J. Stat. Phys. **131**, 567 (2008).

[8] M. Jerkins, M. Schröter, H. L. Swinney, T. J. Senden, M. Saadatfar, and T. Aste, Phys. Rev. Lett. **101**, 018301 (2008).

[9] R. Pal, Polym. Eng. Sci. **48**, 1250 (2008).

[10] G. Lois, J. Blawzdziewicz, and C. S. O'Hern, Phys. Rev. Lett. **102**, 015702 (2009).

[11] R. Zallen, *Physics of Amorphous Solids* (Wiley, New York, 1983).

[12] C. S. O'Hern, L. E. Silbert, A. J. Liu, and S. R. Nagel, Phys. Rev. E **68**, 011306 (2003).

[13] C. S. O'Hern, L. E. Silbert, A. J. Liu, and S. R. Nagel, Phys. Rev. E **70**, 043302 (2004).

[14] I. M. Krieger and T. J. Dougherty, Trans. Soc. Rheol. **3**, 137 (1959).

[15] A. Dörr, A. Sadiki, and A. Mehdizadeh, J. Rheol. **57**, 743 (2013).

[16] R. K. McGeary, J. Am. Ceram. Soc. **44**, 513 (1961).

[17] S. Torquato, T. M. Truskett, and P. G. Debenedetti, Phys. Rev. Lett. **84**, 2064 (2000).

[18] A. R. Kansal, S. Torquato, and F. H. Stillinger, J. Chem. Phys. **117**, 8212 (2002).

[19] R. Al-Raoush and M. Alsaleh, Powder Technol. **176**, 47 (2007).

[20] K. Lochmann, L. Oger, and D. Stoyan, Solid State Sci. **8**, 1397 (2006).

[21] H. J. H. Brouwers, Phys. Rev. E **74**, 031309 (2006).

[22] T. Okubo and T. Odagaki, J. Phys.: Condens. Mater. **16**, 6651 (2004).

[23] P. Richard, L. Oger, J. P. Troadec, and A. Gervois, Euro. Phys. J. E **6**, 295 (2001).

[24] B. R. Aïm and L. P. Goff, Powder Technol. **1**, 281 (1967).

[25] H. Y. Sohn and C. Moreland, Can. J. Chem. Eng. **46**, 162 (1968).

[26] A. R. Dexter and D. W. Tanner, Nature **238**, 31 (1972).

[27] W. M. Visscher and M. Bolsterli, Nature **239**, 504 (1972).

[28] D. M. E. Thies-Weesie and A. P. Philipse, J. Colloid Interface Sci. **162**, 470 (1994).

[29] A. Donev, S. Torquato, F. H. Stillinger, and R. Connelly, J. App. Phys. **95**, 989 (2004).

[30] A. Donev, F. H. Stillinger, and S. Torquato, Phys. Rev. Lett. **96**, 225502 (2006).

[31] T. S. Hudson and P. Harrowell, J. Phys. Chem. B **112**, 8139 (2008).

[32] W. Schaertl and H. Sillescu, J. Stat. Phys. **77**, 1007 (1994).

[33] M. Hermes and M. Dijkstra, Europhys. Lett. **89**, 38005 (2010).

[34] M. Clusel, E. I. Corwin, A. O. N. Siemens, and J. Brujic, Nature **460**, 611 (2009).

[35] C. C. Furnas, Ind. Eng. Chem. **23**, 1052 (1931).

[36] R. S. Farr and R. D. Groot, J. Chem. Phys. **131**, 244104 (2009).

[37] D. P. Haughey and G. S. G. Beveridge, Can. J. Chem. Eng. **47**, 130 (1969).

[38] M. Subbanna, P. C. Kapur, and Pradip, Ceram. Int. **28**, 401 (2002).

[39] M. Suzuki and T. Oshima, Powder Technol. **44**, 213 (1985).

[40] M. J. Powell, Powder Technol. **25**, 45 (1980).

[41] H. D. Lewis and A. Goldman, J. Am. Ceram. Soc. **49**, 323 (1966).

[42] F. G. Tickell, O. E. Mechem, and R. C. McCurdy, T. Am. I. Min. Met. Eng. **103**, 250 (1933).

[43] N. Xu, J. Blawzdziewicz, and C. S. O'Hern, Phys. Rev. E **71**, 061306 (2005).

[44] W. S. Jodrey and E. M. Tory, Phys. Rev. A **32**, 2347 (1985).

[45] J. Tobochnik and P. M. Chapin, J. Chem. Phys. **88**, 5824 (1988).

[46] A. Donev, S. Torquato, F. H. Stillinger, and R. Connelly, Phys. Rev. E **70**, 043301 (2004).

[47] K. W. Desmond and E. R. Weeks, Phys. Rev. E **80**, 051305 (2009).

[48] G. D. Scott and D. M. Kilgour, J. Phys. D Appl. Phys. **2**, 863 (1969).

[49] G. W. Delaney, S. Hutzler, and T. Aste, Phys. Rev. Lett. **101**, 120602 (2008).

[50] S. D. S. Reis, N. A. M. Araújo, J. S. Andrade Jr., and H. J. Herrmann, Europhys. Lett. **97**, 18004 (2012).

[51] A. Santos, S. B. Yuste, M. López de Haro, G. Odriozola, and V. Ogarko, Phys. Rev. E **89**, 040302 (2014).

[52] W. G. Ellenbroek, E. Somfai, M. van Hecke, and W. van Saarloos, Phys. Rev. Lett. **97**, 258001 (2006).

[53] T. S. Majmudar, M. Sperl, S. Luding, and R. P. Behringer, Phys. Rev. Lett. **98**, 058001 (2007).

[54] A. J. Liu and S. R. Nagel, Ann. Rev. Condens. Matter Phys. **1**, 347 (2010).

[55] K. W. Desmond, P. J. Young, D. Chen, and E. R. Weeks, Soft Matter **9**, 3424 (2013).

[56] G. Katgert and M. van Hecke, Europhys. Lett. **92**, 34002 (2010).

[57] L. Berthier and G. Biroli, Rev. Mod. Phys. **83**, 587 (2011).

[58] P. Chaudhuri, L. Berthier, and W. Kob, Phys. Rev. Lett. **99**, 060604 (2007).

[59] G. L. Hunter and E. R. Weeks, Rep. Prog. Phys. **75**, 066501 (2012).

[60] E. Marcotte, F. H. Stillinger, and S. Torquato, J. Chem. Phys. **138**, 12A508 (2013).

[61] Z. Zhang, N. Xu, D. T. N. Chen, P. Yunker, A. M. Alsayed, K. B. Aptowicz, P. Habdas, A. J. Liu, S. R. Nagel, and A. G. Yodh, Nature **459**, 230 (2009).